

## Investigating the tribological and biological performance of covalently grafted chitosan coatings on Co–Cr–Mo alloy



Liguo Qin<sup>a,\*</sup>, Xinan Feng<sup>a</sup>, Mahshid Hafezi<sup>a</sup>, Yali Zhang<sup>b</sup>, Junde Guo<sup>a</sup>, Guangneng Dong<sup>a,\*\*</sup>, Yuanbin Qin<sup>c</sup>

<sup>a</sup> Key Laboratory of Education Ministry for Modern Design & Rotary-Bearing System, Xi'an Jiaotong University, Xi'an, 710049, PR China

<sup>b</sup> Key Laboratory of Biomedical Information Engineering of Ministry of Education, School of Life Science and Technology, Xi'an Jiaotong University, Xi'an, 710049, PR China

<sup>c</sup> Center for Advancing Materials Performance from the Nanoscale, State Key Laboratory for Mechanical Behavior of Materials, Xi'an Jiaotong University, Xi'an, 710049, PR China

### ARTICLE INFO

#### Keywords:

Co–Cr–Mo alloy  
Chitosan coatings  
Tribology  
Bioactive

### ABSTRACT

A layer-by-layer deposition technique with grafting chitosan on the Co–Cr–Mo alloy was developed. The performance of tribology and biocompatibility were investigated under simulated conditions. Wettability of coating surface was super hydrophilic and the surface was in positive charge under the neutral solution, which was favored in water-based lubricating and adhesion of cells. By pin-on-disk tests, the chitosan coating surface exhibited lower friction coefficient under various sliding speed as compared with the uncoated substratum. A wear rate of  $1.1 \times 10^{-7} \text{mm}^3/\text{Nm}$  was detected, which was only one seventh of uncoated surfaces. Hypothetically illuminating the mechanism of antifriction is able to lead for better wear resistance. Co-culturing with osteoblast cells showed that coating had good benefits in the proliferation of osteoblast cells.

### 1. Introduction

Loading bearing implants, such as the total hip and total knee replacements have been paid extensive consideration among clinicians. It is caused to the tremendous increment in patients who are suffering from arthritis and joint related issues. As one of the most important cobalt alloys, Co–Cr–Mo alloy has been widely used in various biomedical applications, such as the dental and hip joint implants (e.g., the metal on metal (MOM) hip joint). Impressive properties of Co–Cr–Mo alloy include excellent mechanical behavior, brilliant corrosion resistance and biocompatibility [1–3]. However, natural hip joints are lubricated by synovial fluid, the MOM joints are exposed to be lubricated by a mixture of blood and body fluids during their early post-operative period. There are numerous reports indicating that the debris produced by this prosthesis is inevitable, leading to inflammation of tissues and causing aseptic loosening of joints [4]. Wear mechanisms were classified into abrasive, adhesive, fatigue, fretting and corrosive as conducted by previous studies [5,6]. To overcome these problems, several surface modification techniques, such as plasma treatment [7], surface texturing [8–10] and appropriate hard coatings [11], have been developed to reduce the friction force and improve the wear resistance.

Inspiring from nature soft tissue of articular cartilage, which coats the sliding surfaces of joints, presents some of the greatest challenges to our understanding. The articular cartilage is capable of highly lubricated sliding over a wide range of shear rates. The hyaluronic acid and aggrecan system is an example of a topologically complex structure, which is particularly fruitful for the strategy in the field of wear protection and lubrication. Even though it is under question mark that such surface truly be able to act like the articular cartilage and provide efficient lubrication. Coating bio-macromolecules or soft molecules on biomaterials has been increased attentions particularly in biotribology. Chitosan is a linear cationic polysaccharide that is derived from chitin by partial deacetylation [12]. In addition the low toxicity, biocompatibility and biodegradability, chitosan is famous to display antibacterial, hypoallergenic, wound healing, and film forming properties [13,14]. It is regard as the one of the most widely researched natural polymer based system for biomedical applications.

Poor mechanical strength of bonding is the limitation of chitosan used as coatings on metal surface. This is because the metal surface (e.g., titanium and cobalt) became highly unreactive through a process called passivation [15]. The passivation limited the bonding ability of metallic implants with biologic coatings. Several surface activation

\* Corresponding author.

\*\* Corresponding author.

E-mail addresses: [liguoqin@xjtu.edu.cn](mailto:liguoqin@xjtu.edu.cn) (L. Qin), [donggn@mail.xjtu.edu.cn](mailto:donggn@mail.xjtu.edu.cn) (G. Dong).

techniques were used, such as plasma and etching. Recently, the layer-by-layer deposition has attracted much attention for functionalizing the inert surface because it is facile, versatile and efficient [16]. Feng showed that polyelectrolytes multilayer films using a time- and cost-efficient spin-assisted layer-by-layer self-assembly technique provided much better frictional properties than the silicon substrate [17].

Therefore, using the layer-by-layer technique to graft chitosan on Co–Cr–Mo alloy is wisely decision. This approach provided a method to maintain the bioactivity of chitosan without losing appropriate wear protection and lubrication. In order to evaluate potential tribology and biocompatibility properties, the microstructure, mechanical, frictional and biocompatibility properties of chitosan coatings were evaluated.

## 2. Material and methods

### 2.1. Materials

Commercially available Cobalt–chromium–Molybdenum (Co–Cr–Mo) alloy (ASTM F75, Steel Material Technology Co., Ltd., China) was used as received and contained the follow elements: C ( $\leq 0.35\%$ ), Mn ( $\leq 1.0\%$ ), Si ( $\leq 1.0\%$ ), Cr (26–30%), Ni ( $\leq 1\%$ ), Fe ( $\leq 0.75\%$ ), Mo (5.0–7.0%), Co (balance) and N ( $\leq 0.25\%$ ). In a typical procedure, all the prepared surfaces were produced in the same process. The detailed process was given as follows. The dimension of specimen was 12 mm  $\times$  6 mm  $\times$  2.5 mm. One 12 mm  $\times$  6 mm surface was polished to mirror finish using a series of sand grinding papers up to 1600 grit. Then it was ultrasonic cleaned in ethanol and distilled water, following by drying in atmosphere. The surface roughness (Ra)  $\sim$  80 nm was measured by a surface profiler (TR-200, Time Group) in a scanning length of 1.2 mm, which was consisted with the surface finish of the commercial hip joint replacements. Finally, samples were sterilized in 120 °C water steam for 20 min, and then dried at 90 °C for 1 h for future use.

The high purity chitosan (110 kDa,  $\sim$ 75% deacetylated), 3-ammonium propyl triethoxy silane (APTES), glutaraldehyde (GA), Dulbecco's modified Eagle's medium (DMEM), Bovine serum albumin (BSA), dimethylsulfoxide (DMSO) and 3-(4, 5-dimethylthiazol-2-yl)-2, 5-diphenyltetrazolium bromide (MTT) were obtained from Sigma (St. Louis, MO, USA); Fetal Bovine Serum (FBS, Gibco, UK) was purchased from Gbico (Paisley, UK).

### 2.2. Fabricating chitosan coatings

Chitosan coatings were prepared via the layer-by-layer deposition process. Fig. 1 shows schematic procedures for fabricating chitosan coatings on Co–Cr–Mo alloy. First treatment (step 1) was hydroxylation. Pretreated Co–Cr–Mo alloy was immersed into piranha solution (7:3 (v/v) mixture of 98% H<sub>2</sub>SO<sub>4</sub> and 30% H<sub>2</sub>O<sub>2</sub>) for 20 min, placed in a ultrapure water bath for 24 h and rinsed at least four times with ultrapure water (samples denoted as Co–OH). Dried Co–OH was submerged in a fresh prepared solution containing 2% (v/v) APTES, 5% (v/v) deionized water and 93% (v/v) acetone for another 60 min (step 2). The samples were sequentially rinsed with acetone and deionized water, and dried (samples denoted as Co–APTES). As shown in the step 3, Co–APTES was treated with 2% (v/v) glutaraldehyde (GA) in ultrapure water overnight at 25 °C under slow agitation (50 rpm). Each sample was rinsed thrice with deionized water for 1 min (samples denoted as Co–GA). Co–GA samples were immersed in the solution containing 1 wt% chitosan, 1 wt % acetic acid, and 98 wt % deionized water for 12 h. After adjusting the pH to 7.0, the samples were rinsed with deionized water and dried at room temperature (samples denoted as Co–CS). In biological assessment, coating samples were sterilized by ultraviolet radiation for 5 h.

### 2.3. Surface characterization

SU6300 scanning electron microscopy (JEOL, Japan) with an

Oxford Inca energy dispersive X-ray microanalysis (EDX) operating at 20 kV was used to observe the microstructure and morphologies of the samples. 3D topographic details were obtained using an Innova Digital Nanoscope AFM (Veeco, America) in tapping mode. Commercial silicon cantilever probes (RTESP, Bruker) with a spring constant of 0.35 N/m and a nominal tip radius of 8 nm were used. The scanning area was 1  $\mu$ m  $\times$  1  $\mu$ m and the scanning rate was 0.8 Hz. The chemical composition and bonding configurations were collected from an Ultra XPS spectrometer (Surface science). The spectrometer had a monochromatic Al K $\alpha$  X-ray source operating at 15 kV and 10 mA (150 W) for all data acquisitions and XPS peaks were analyzed using the XPSPEAK 4.1 software.

Contact angle measurement was performed using a JC2000DA video-based optical system (Digital technology equipment Co., Ltd., China). DMEM droplets, volume 5  $\mu$ L, were dropped on materials through a goniometer with an outer diameter of 0.5 mm at ambient temperature. Images of water spreading on the sample were recorded by a camera, and then analyzed using the software supplied by the manufacturer. Duplicate measurements were obtained on different areas of each sample. Three samples were measured in each group.

Zeta potentials provided a unique method to quantify the actual state of the interface between the solid and the solution. Zeta potential studies were performed using a streaming potential instrument (Surpass Electrokinetic Analyzer, Anton Paar, Austria). A cell with adjustable gap was used to determine apparent  $\zeta$ -potential of different functionalized surfaces. The procedure has been described in detail previously [18]. A standard KCl solution (1 mM) was used as electrolyte. The pressure ramp was run up to a maximum pressure of 200 mbar. For each surface condition, four measurements were performed.

### 2.4. Mechanical characterization

Nano-indentation was applied to reveal mechanical properties i.e. hardness and elastic modulus of the coatings. The instrument monitors and records dynamic load and displacement of three-sided pyramidal diamond Berkovich indenter during indentation with a force resolution of approximately 75 nN and displacement resolution of approximately 0.1 nm. Experiments were performed at clean air environment and 23 °C ambient temperatures.

### 2.5. Friction measurements

Frictional performances were investigated using a pin-on-disc tribometer (UMT-2, CETR Corporation Ltd, USA) in reciprocating sliding. The upper Co–Cr–Mo sample was pin with the diameter of 2 mm and length of 4 mm. Co–Cr–Mo alloy disc was loaded to reciprocate on a horizontal plane. The reciprocating stroke length was adjusted to 6 mm. As shown in Fig. 2, all tests were carried out under the following conditions: 2.4 MPa of the contact pressure at air atmosphere, room temperature and relative humidity about 40%. Lubricants were BSA with the concentration of 2 mg/ml. Coefficient of friction (COF) was automatically recorded. The worn surfaces were observed by SEM.

### 2.6. Cell viability and morphologies

In vitro biological tests were performed using the standard cytotoxicity tests (ISO 10993–5) with the immortalized mouse calvarium osteoblast-like cell (MC3T3-E1). The cells were cultured in DMEM containing 10% Foetal Bovine Serum, penicillin/streptomycin (1%, GIBCO, UK) and Hepes (2%, Invitrogen, UK), then incubated at 37 °C, 5% CO<sub>2</sub> atmosphere and 100% relative humidity. For subculture, the single layer cell was washed twice with phosphate-buffered saline and incubated with trypsin-EDTA solution (0.1% trypsin, 0.25% EDTA) for 10 min at 37 °C to detach cells. The medium was changed every 1–2 days. Cultures were evaluated for cell viability/proliferation at 6, 24 and 48 h (MTT assay) and cell morphologies were observed by SEM.

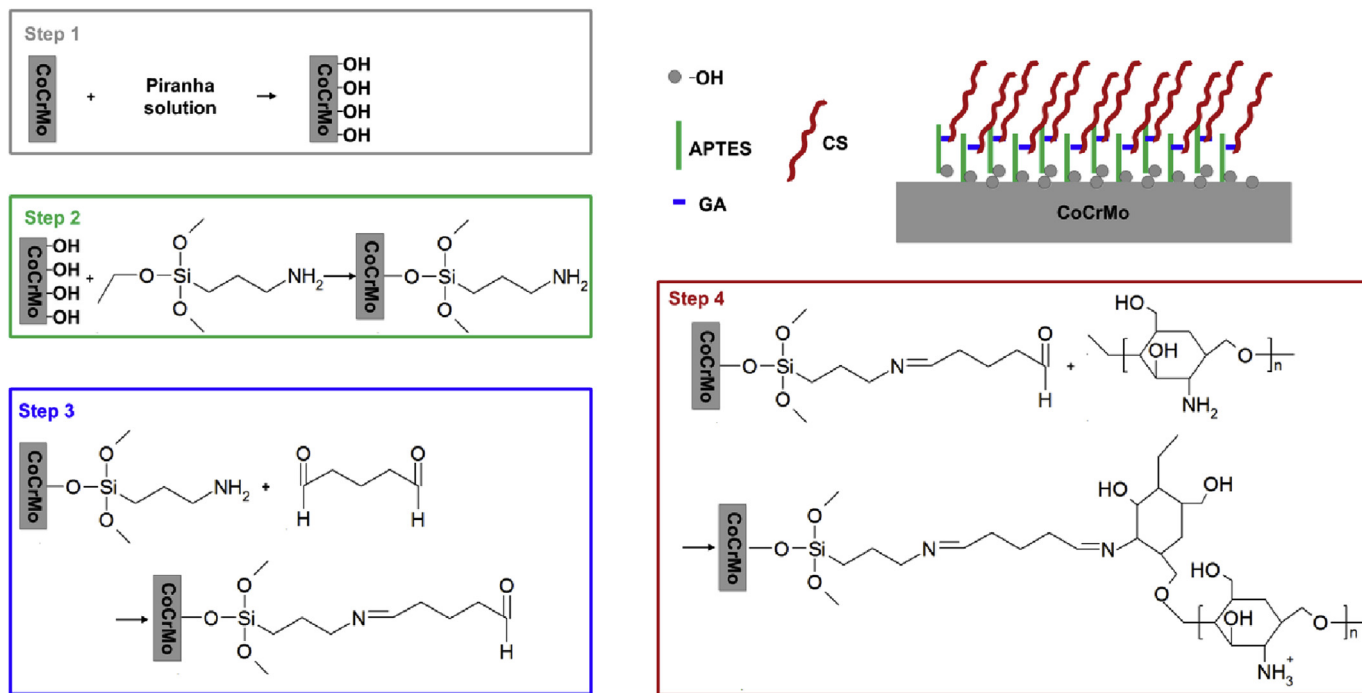


Fig. 1. Process of grafting chitosan covalently to Co–Cr–Mo via the layer-by-layer technique.

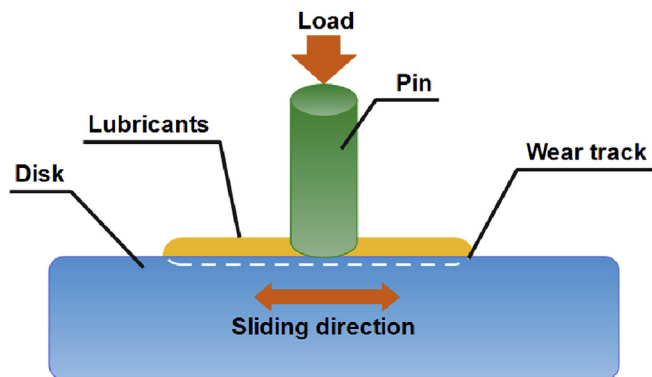


Fig. 2. Schematic diagram of the tribosystem.

### 3. Results and discussion

#### 3.1. Surface morphology

Representative morphologies of various samples are shown in Fig. 3. Surfaces were polished smoothly and just several superficial scratches were left (Fig. 3a). The contamination and white particles were disappeared after treated with piranha solution and a favorable surface containing oxygen groups was fabricated, which was suitable for the following process of layer-by-layer coating (Fig. 3b). Fig. 3c shows the

SEM image of CS coatings on the Co–Cr–Mo substrate, exhibiting a branch-like morphology characteristic of components based on chitosan molecules and with surface roughness ( $R_a$ ) of  $0.81 \pm 0.13 \mu\text{m}$ . The coating surface exhibited more rough morphology as compared to the polished surface, which is desirable to improve the biocompatibility of the biomaterials. Previous studies have illustrated the roughness in combination with the presence of a bioactive layer or interface could have a synergic effect and may be responsible for improvement in cell colonization or proteins adsorption in a material.

Detailed topographies of Co–CS under dry and wet condition were characterized by AFM, as shown in Fig. 4. When the coated surface was totally dried, the vertical height measured from cross section was in the range of  $-4 \sim 8 \text{ nm}$ , while it was significantly decreased and exhibited  $1/3$  value from  $0 \sim 3.8 \text{ nm}$  at the wet condition. Due to the electrolytic dissociation, repulsive force was dominated to make the outmost chain of CS molecule alignment. Highly oriented layers were formed and giving a more smooth roughness (RMS was decreased from  $4.2 \text{ nm}$  to  $1.8 \text{ nm}$ ). It was reported that surfaces with more ordered and aligned chains could provide higher load capacity, be able to decrease the shearing force and improve the wear resistance. Morphologies of Co–Cs surfaces have indicated good lubricating property specifically under wetting condition.

#### 3.2. XPS characterization

Fig. 5a showed the XPS survey spectrum of Co–Cr–Mo and Co–CS,

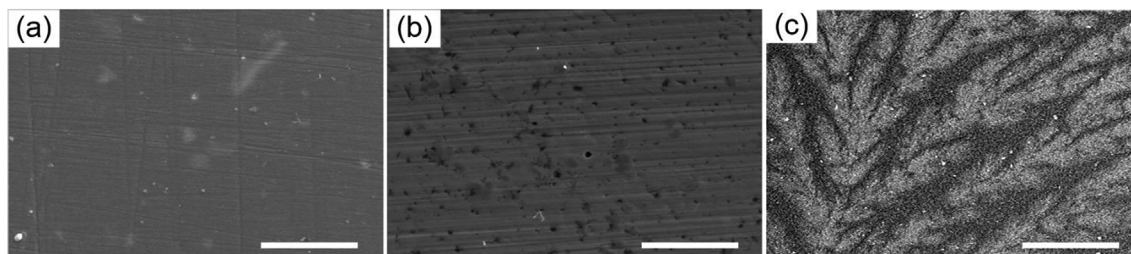


Fig. 3. SEM images of (a) Co–Cr–Mo, (b) Co–OH and (c) Co–CS. The scale bar is  $40 \mu\text{m}$ .

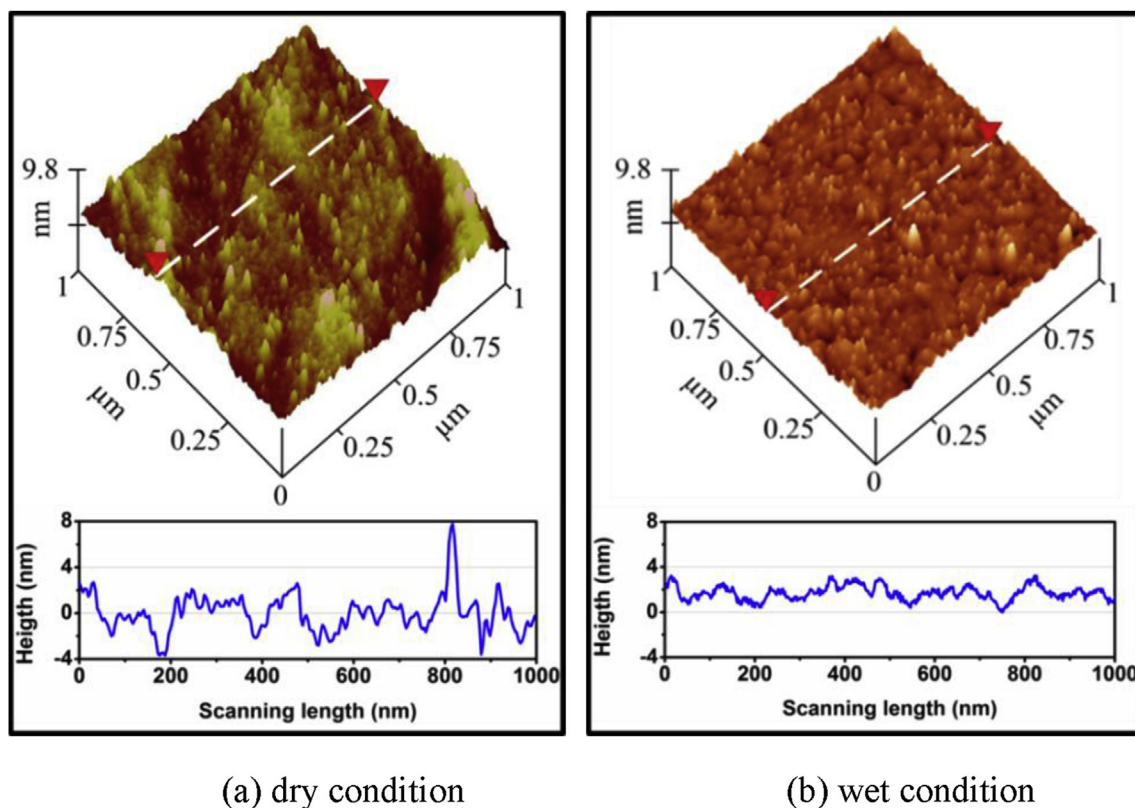


Fig. 4. AFM topography of CS coating under dry and wet condition.

respectively. It was noted that intensity of metal peaks for Co–CS, such as cobalt (Co 2p), chromium (Cr 1s) and molybdenum (Mo 3d), were decreased. The distinct peak (around 400 eV) on the survey spectrum of Co–CS was attributed to N 1s, denoting the successful grafting of CS molecules on the substrate. A broad main peak at 284.6 eV and chemically shifted peak at 288.2 eV was resolved for aliphatic carbon [19], while the C 1s spectrum was decomposed into three peaks ranging from 278 eV to 293 eV, assigning to C–H or C–C (284.4 eV), C–O (285.9 eV), after CS grafting [20]. The analysis of O 1s peaks, Fig. 5c, revealed one extra contribution for CS coating surface, 532.3 eV for C–O [21]. The grafting treatment incremented the intensity of hydroxyl group and decreased the intensity of oxides. As shown in Fig. 5d, nitrogen peaks were not detected on the surfaces of Co–Cr–Mo. De-convolution of N 1s peak resulted in two sub-peaks at 399.5 eV and 401.4 eV, individually. The two peaks were assigned to amine and amide groups [22]. These results proved that CS molecules were covalently grafted on Co–Cr–Mo alloy with strong adhesion between substrate and layers.

### 3.3. Mechanical characteristic

Mechanical properties of Co–Cr–Mo and Co–CS at the nano scale were surveyed by nano-indentation technique. Fig. 6 presents the load–displacement curves under linearly enhancement load from 0 to 2000  $\mu\text{N}$ . Under the load of 2000  $\mu\text{N}$ , the maximum displacement for Co–Cr–Mo was 91.8 nm. After coating, this value was significantly increased. A value of 540.8 nm was observed for Co–CS in dry condition, while this value was slightly decreased to 493.4 nm for Co–CS in wet condition. It was mainly caused by the repulsive force, which was produced during the process of electrolytic dissociation. Moreover, such a repulsive force may keep the surfaces apart under high load.

The hardness (H) and elastic modulus (E) were shown in Table 1. For samples without coating, highest stiffness, hardness and elastic modulus were observed. After coating, these parameters were sharply decreased. For the coating in dry condition, the stiffness was the lowest

(5.2  $\mu\text{N}/\text{nm}$ ), which was about 1/19 of the polished Co–Cr–Mo. As compared to the polished Co–Cr–Mo, H fell down by 80%, 1.3 GPa. E value for Co–CS was 4.5 GPa and 1/40 of Co–Cr–Mo. When it was in wet condition, the hardness was not changed and the E value was slightly increased. The H/E ratio was the highest for Co–CS in wet condition. Based on the Bowden-Tabor theory, the COF would be significantly decreased and lower value would be achieved when soft coatings were fabricated on the rubbing surfaces. Generally, hardness has been regarded as primary material property that defines wear resistance. There is strong evidence to suggest elastic modulus also has an important influence on wear behavior. Particularly, the elastic strain to failure is related to the ratio of H and E. Leyland [23] mentioned the elastic strain to failure could be a more suitable parameter for predicting wear resistance than hardness. Researchers [24–26] demonstrated that ratio of H to E in terms of ‘plasticity index’ or ‘elastic strain to failure’ were widely described as valuable parameter in determining the limit of elastic behaviors in surface contact, truly important for lowering wear. H/E value was calculated as 0.289 for CS coatings in dry condition where the typical value for Co–Cr–Mo was 0.044. This ratio was even increased to 0.329 for CS coatings in dry condition. It was accepted CS coating may provide superior wear resistance although the hardness was not extremely high, especially in wet condition. At the same time, cells were highly active when they were seeded on substrates with comparative hardness and Elastic modulus (less stress shielding). In this survey, the fabricated CS coating specially dropped the hardness and Elastic modulus of Co–Cr–Mo substrate. Potential application in orthopedic implants, e.g. osseointegration, would be considered.

Micro-Scratch tests were performed at room temperature according to ASTM D7027-13. As shown in Fig. 7 (a), the scratch load was increased linearly from 0 mN to 5 mN at a constant speed of 0.33 mN/s over a distance of 5 mm. The apparent lateral force versus linearly increasing normal load was shown in Fig. 2 (b). For the physical grafted CS, several fluctuations of lateral force were observed when the load

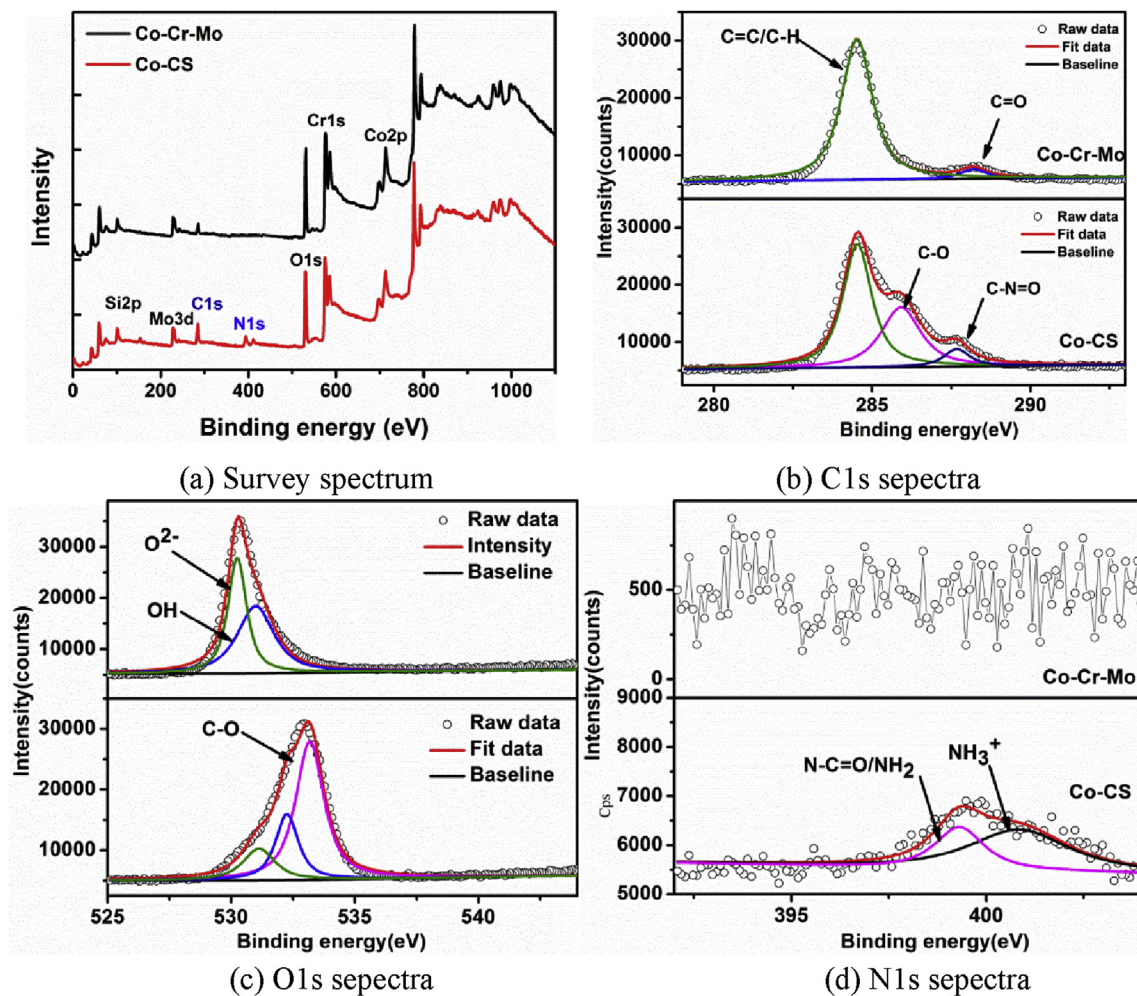


Fig. 5. XPS survey spectra and high resolution spectrum of C 1s, O 1s and N 1s.

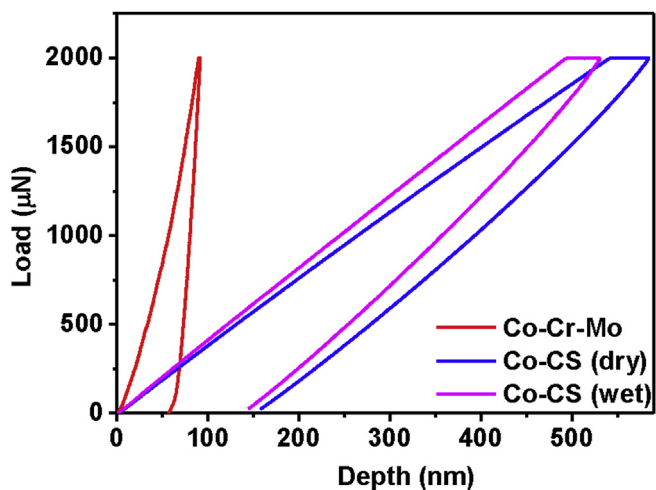


Fig. 6. Nano-indentation of Co–Cr–Mo and Co–CS under dry and wet condition.

was over 1.8 mN. The lateral force was almost decreased to zero at the load around 3.8 mN, which demonstrated the adhesion force was less than 4 mN for the physical grafted CS. For the chemical grafted CS, the lateral force was nearly linear to the load during the whole scratch process. It indicated a stable coating with a strong scratch resistance over 5 mN was achieved by the covalently grafting method.

Table 1  
Parameter of Mechanical properties.

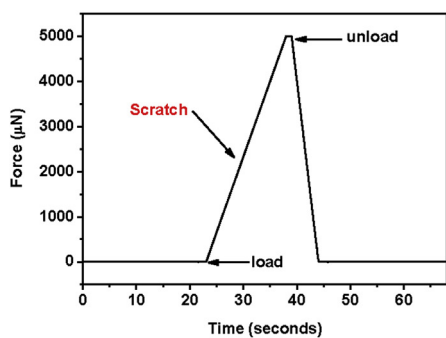
Sample	Stiffness (N/nm)	Nano-hardness (H, GPa)	Elastic modulus (E, GPa)	H/E
Co–Cr–Mo	98.7	7.9	178.5	0.044
Co–CS (dry)	5.2	1.3	4.5	0.289
Co–CS (wet)	5.5	1.3	3.9	0.329

### 3.4. Surface wettability

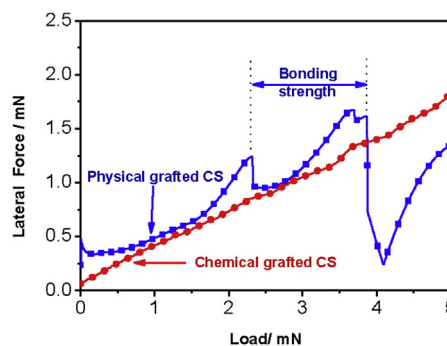
After each processing level, the contact angle was measured. As shown in Fig. 8, the polished sample showed the highest contact angle, 48°. By hydroxylation, the contact angle was 16° due to the surface functionalized with –OH group, which had higher affinity to the water. After deposited with APTES, the contact angle was 30°. For Co–CS, the contact angle could not be measured. It was super-hydrophilic. Surface roughness and wettability of an implant material are among the most important parameters that influencing protein adsorption dynamics therefore cell adhesion and proliferation. In fact low contact angle value (i.e. high surface energy) is able to promote greater cell adhesion compared to a high contact angle value [27].

### 3.5. Zeta potential

Fig. 9 shows the zeta potentials for functionalized and native Co–Cr–Mo surfaces at pH 7. The difference between electrical



(a) the load profile



(b) the lateral force verse the load

Fig. 7. The micro scratching process and the lateral force versus applied normal load for physical and chemical grafted CS.

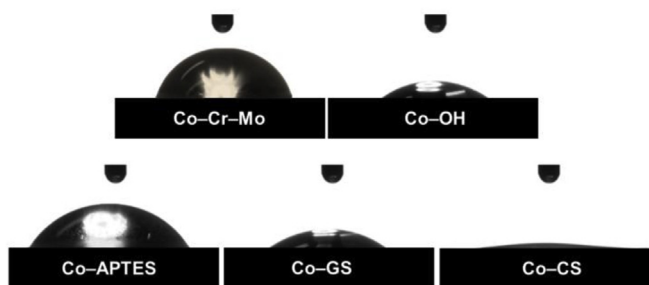


Fig. 8. Contact angles for different samples.

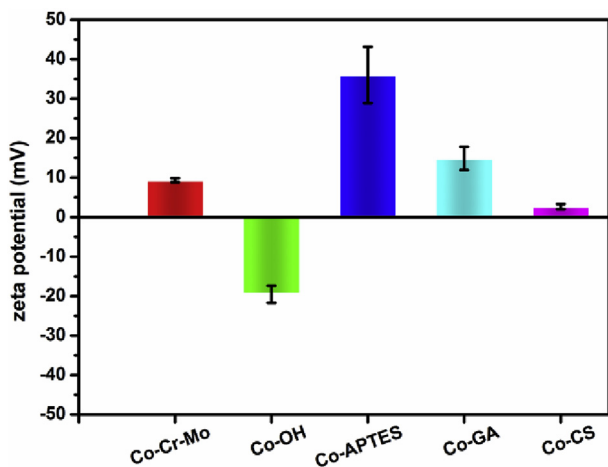


Fig. 9. Zeta potentials at pH value of 7.0. Different zeta potentials regarding native Co-Cr-Mo and surface functionalized with different functional end molecules were observed. Four measurements were performed for each sample.

properties of surfaces was observed clearly. The absolute zeta-potential was compared consecutively: Co-CS < Co-Cr-Mo < Co-GA < Co-OH < Co-APTES. Polished Co-Cr-Mo was found to be positively charged. The piranha treated surface was the most negative surface at physiological pH. Evidences showed the detection of hydroxyl groups by XPS was the effective reason. The charge reversal was observed for Co-APTES. Large amounts of protonated  $\text{NH}_3^+$  groups continuously reacting with GA, zeta potential decreased along with consuming amino groups. Although chitosan had a lot of monomers containing amino groups, the pKa value of its amino group was 6.2–6.8 [28]. Therefore zeta potential of Co-CS was negligible positive ( $2.6 \pm 0.7$  mV) at neutral pH. Zeta potential as surface charge has greatly influence on the alignment of chains in solution through the electrostatic repulsion. It can also effect the surface interaction in vivo with the cell membrane, which is usually negatively charged.

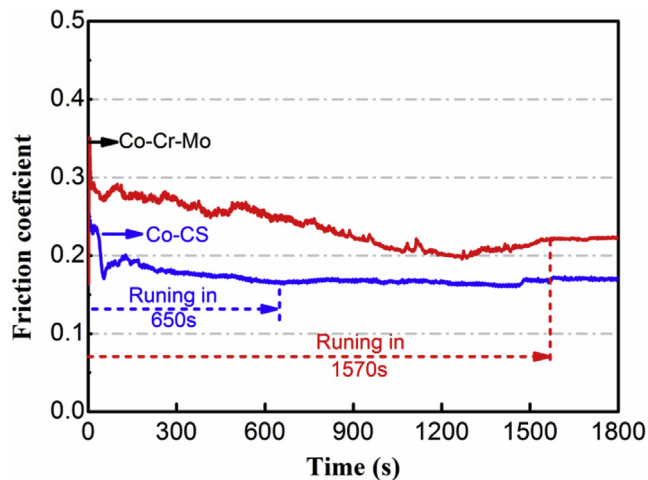


Fig. 10. Friction coefficient of CS coating surface.

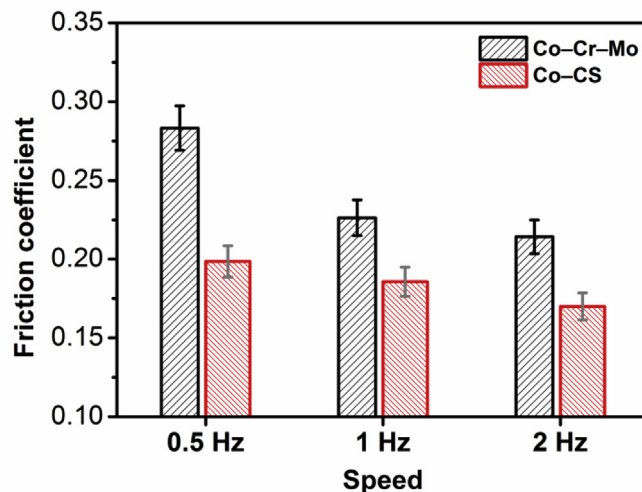
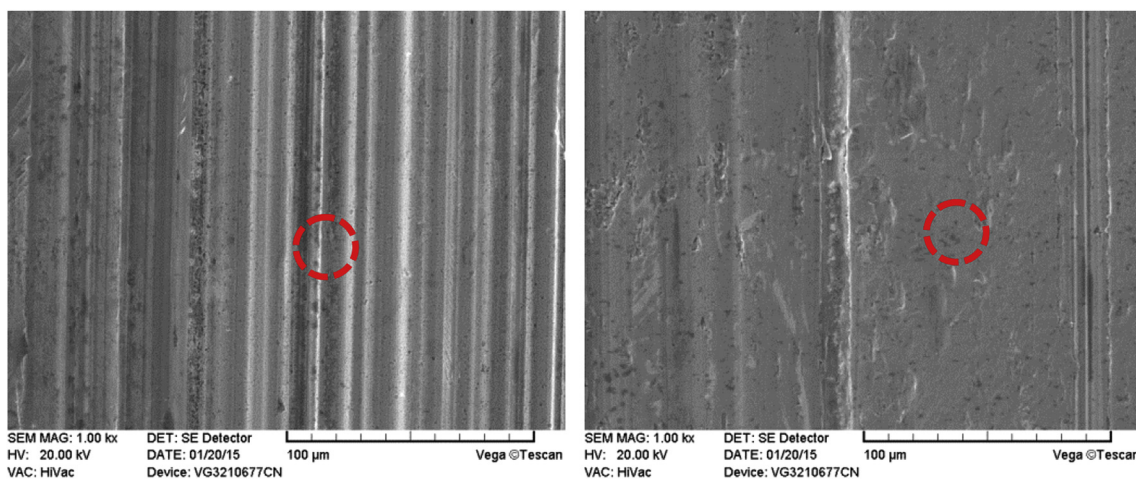


Fig. 11. Friction coefficient varied with sliding velocity.

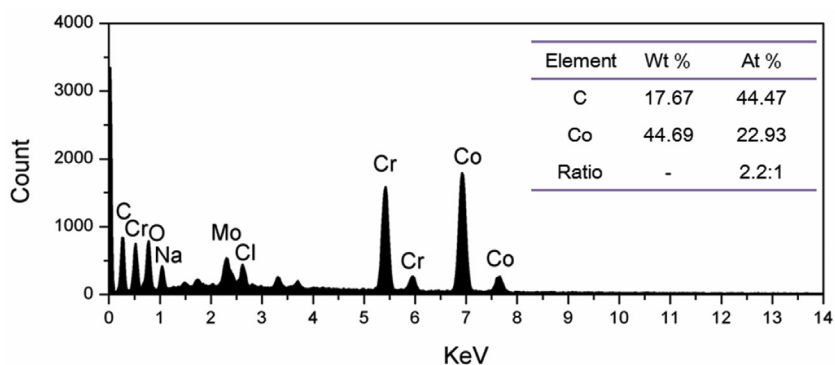
### 3.6. Friction measurements

Average COF for CS coating surface was around 0.18 as shown in Fig. 10. It decreased by 40% as compared with the polished Co-Cr-Mo surface. The sliding process for surface coated with CS layer was less vibration taking 650 s to the steady-stable state, while the sliding time was about 1570 s for the polished surface to reach the steady-stable state. The running-in period is critical for the life of metal-on-metal hip

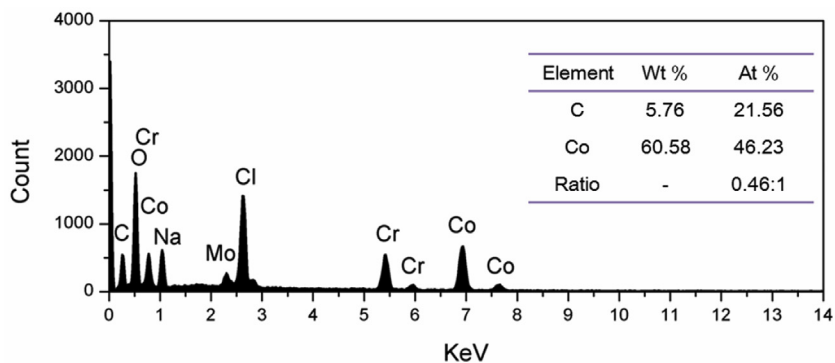


(a) Co–Cr–Mo

(b) coating surface



(c) EDS spectrum of red marked area in (a)



(d) EDS spectrum of red marked area in (b)

Fig. 12. SEM images and EDS spectrum of worn surface.

joints. The wear rate in running-in period is higher than steady state due to the generation of third body particles from exposed asperities fracturing during running-in period [23–25,29]. Intelligibly short running-in can decrease the amount of wear particles [30].

Fig. 11 shows the COF of substrates under different sliding velocity. It was found COF decreased for both of polished and coating surface while sliding velocity was increased. When the velocity was 0.5 Hz, the highest COF on polished sample was noted. Under a velocity of 2 Hz, the coating surface exhibited the minimum COF of 0.17. It detected improving performance of lowering COF for CS coatings specifically under increasing sliding velocity.

### 3.7. Wear resistance

After frictional test, the worn surface was cleaned using distilled water and then observed under the SEM microscope. Fig. 12 a showed the worn surface morphologies after tribotest for 30 min. The worn ploughs of coating surface were much slighter than polished surface (Fig. 12b). More microscopic undulations were observed on polished Co–Cr–Mo surface. It was also found that ploughs of coating surface were smoother than polished surfaces. The EDS spectrum of rubbing surface showed ratio of C to Co for coating surface were much higher than polished surface. The C element was mainly derived from CS

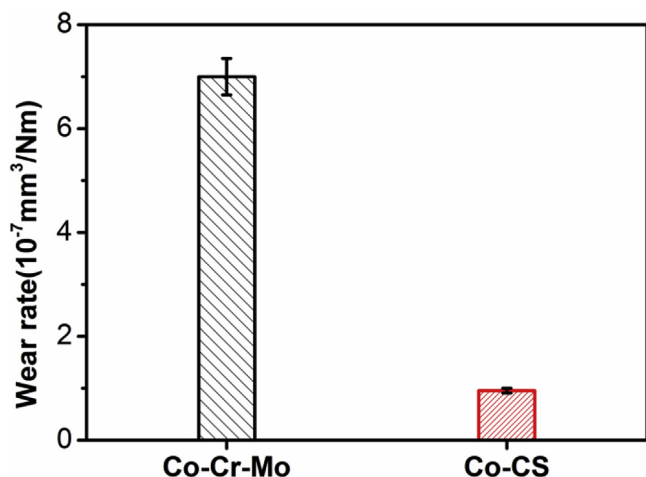


Fig. 13. Wear rate of polished and coated Co–Cr–Mo surface.

coatings, which protected the surface from direct contact and reduced the abrasive wear.

For quantifying the wear resistance of coating sample, the speeding wear test was performed. The pin was replaced by the Co–Cr–Mo alloy ball with a radius of 9.5 mm. The frequency of 1 Hz was used and the stroke was 6 mm. The same load was considered and the initial Hertz contact pressure was 1.2 GPa. The wear rate for the CS coated surface was  $1.1 \times 10^{-7} \text{ mm}^3/\text{Nm}$  and the value for uncoated Co–Cr–Mo was nearly 7 folds of the coated surface, shown in Fig. 13. Simulations revealed that the wear rate of  $8 \times 10^{-7} \text{ mm}^3/\text{Nm}$  yielded average linear wear rate of 0.111 mm/year [31,32]. Evaluating the value of the wear volume, the CS coating may protect the Co–Cr–Mo alloy at least several years from refurbishment which is commonly happened by poor wear resistance.

### 3.8. Mechanism of anti-friction

There are effectively two interfaces for characterizing and optimizing the frictional characteristics of layered materials. Interlayer interface is the first and foremost for majority of interfaces lubricated

with these materials. The shearing process will mainly occur between the layers. Secondly, the interface between substrate and lubricant, when the number of layers is reduced at the interface, becomes increasingly important. Microstructural morphology and chemistry are the most important factors that raise issues of coating conformity and molecule orientation. Numbers of researchers studied grafting polymer entities such as amphiphilic block copolymers onto bare or plasma-treated PDMS substrates. Amphiphilic block copolymers provided effective aqueous lubrication through a hydrated polymeric film that was able to build the steric barrier for asperity contact [33,34]. Similar findings showed PEG was strongly bonded to negatively charged oxide surfaces. The COF was dramatically decreased under boundary lubrication as the polymer was extended and highly solvated.

Macromolecular chain mobility and entanglement are well known to be affected by the presence of potential difference [35]. According to Luo [36], if potential difference was formed between lubricant film and substrate, the polar functional groups in the lubricant molecule would be oriented and interactions between polar groups were modified accordingly. In this study, Co–CS showed a positive charge which explained likely forming an aligned charged chaining surface. Fig. 14 shows the assumed view of the shearing process of disk and ball under different lubrication condition. When CS was covalently grafted on the surface, CS chains were attracted toward the upper/lower surfaces due to the attraction from amino  $\text{NH}_3^+$  groups. Highly ordered chains made the ball slide easily. As a result, the ball was isolated from the disk and friction was occurred mainly on hydrocarbon ( $\text{CH}_2$ –C) ends. While CS molecules were physically adsorbed on the rubbing surface (e.g. CS mixed with the lubricant), they were easily aggregated exhibiting a disorder alignment. The disorder CS could not provide enough load support. Friction force could increase due to the asperity contact. A similar conclusion for potential effect on the attraction of polar group for steel substrate had been published in several studies [35,37,38].

Verify the effect of covalently grafted CS on friction reduction. Experiments with CS contained lubricants were performed. 2 mg/mL BSA was mixed with CS and two concentrations were used 5% and 10% (wt.). Fig. 15 shows the COF with 5% CS lubrication is nearly the same as the Co–CS. When the concentration is 10%, COF is raised immediately and varied from 0.20 to 0.30 during the sliding process. The value of friction force seemed difficulty to be constant. From the

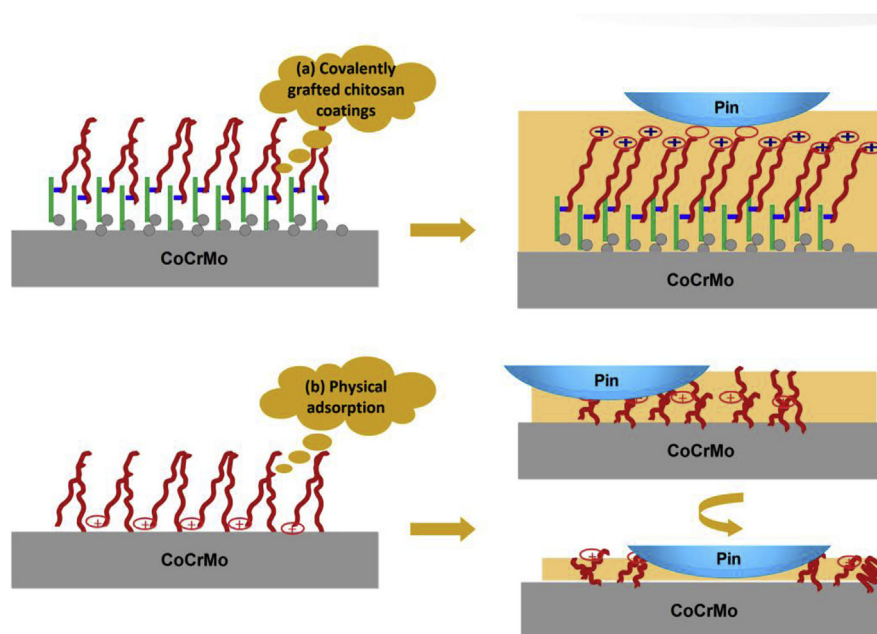


Fig. 14. Two types of shearing process: (a) Chitosan molecules grafted on Co–Cr–Mo surface via layer by layer techniques and (b) Chitosan molecules adsorbed on Co–Cr–Mo surface via physical binding.

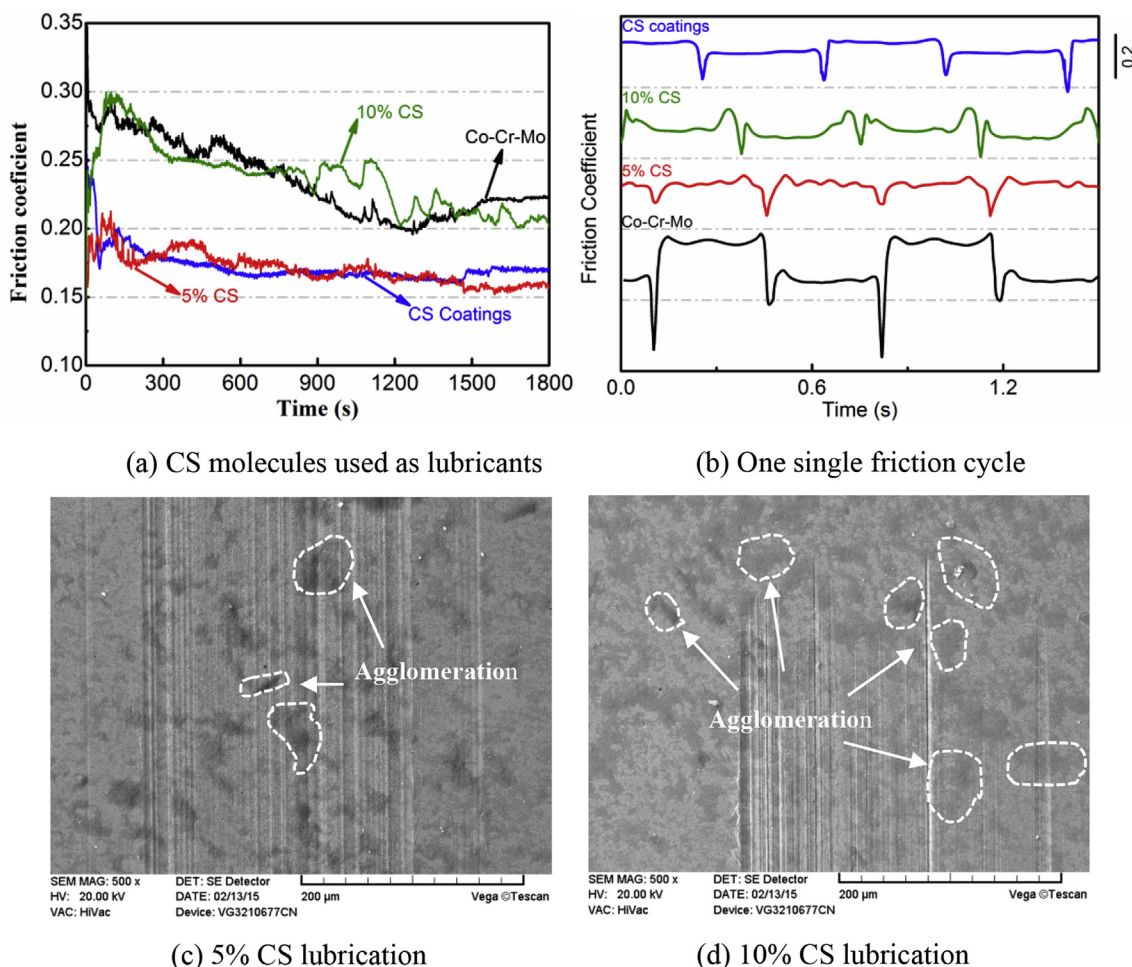


Fig. 15. COF and worn surfaces under CS lubricants with different concentration.

amplified sliding cycle, the Co–CS surface defined more smooth process (e.g. only vibration occurred at the direction change point, and no stick-slip was observed). Partially stick-slip was taken place about 5% CS lubrication, while stick slip was obviously found under 10% CS lubrication. When CS was mixed in lubricants, it was considered that interaction between CS and substrate was physical adsorption. At lower concentration, few parts of CS were in form of agglomeration. With CS concentration exceeded, more agglomeration would be involved. The weak physical adhesion caused CS to be easily separated from the rubbing surface. The worn morphologies and EDS were further approved this assumption. As shown in Fig. 15 (c) and (d), C content of the marked area was increasing with the concentration of CS increasing, while more poor wear resistance was acted.

### 3.9. The proliferation of MC3T3-E1

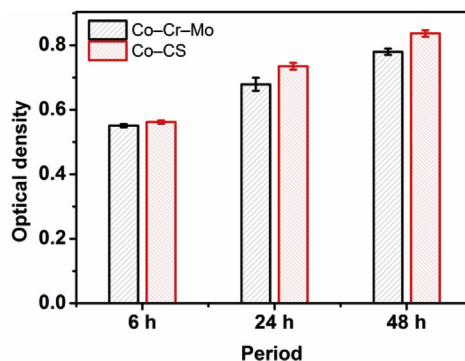
The quantitative analysis of cellular viabilities at as-deposited CS coating was evaluated using the MTT assay. Cell metabolism was measured and the amount of formazan produced was related to the number of living cells. As shown in Fig. 16a, absorbance value for both of coated and uncoated samples was increased from 6 h to 48 h. The absorbance value for Co–CS was significantly larger than the polished Co–Cr–Mo surface. Cell viability of Co–CS had better biocompatibility than Co–Cr–Mo and this effect was emphasized with culture time prolonging. SEM morphology of MC3T3 cells showed the shape of MC3T3 cells was in the normal polygon as reported mostly, while Co–CS exhibited much more spreading area than the Co–Cr–Mo. These confirmed our initial aim to maintain the bioactivity of CS in the layer-

by-layer process. Detail biological assessment will be conducted to reveal the mechanism of good biocompatibility in future studies.

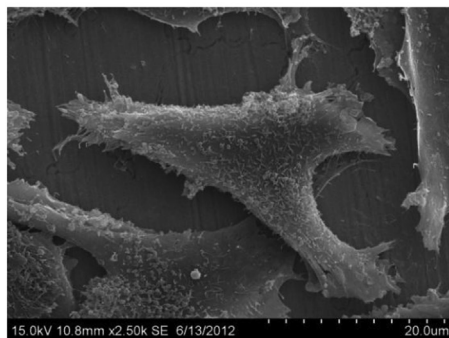
## 4. Conclusions

In this survey, chitosan coating was considered to develop the tribology and biocompatibility performance of the Co–Cr–Mo alloy, one commonly used MOM metal. The following conclusions can be drawn from the results produced above:

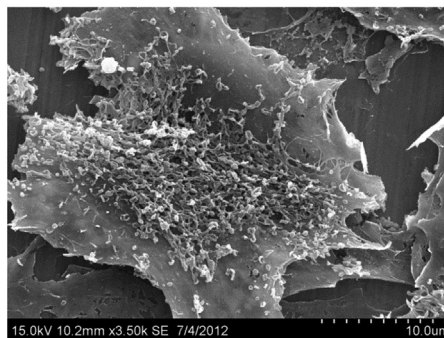
- I) Using layer-by-layer deposition technique, the Co–Cr–Mo alloy was shifted from passivation to activation. Substratum was provided ideally to be modified with functional molecules.
- II) The chitosan was covalently grafted on the Co–Cr–Mo alloy. The process of grafting modification was confirmed by SEM and X-ray photoelectron spectroscopy of the coating surface.
- III) The chitosan coating surface was super-hydrophilic and positively charged. Abatement of surface roughness was observed while transferring from dry to wet condition on the surface. It had lower value of hardness and elasticity modulus while the ratio of H to E maintained with a glorious improvement.
- IV) Chitosan coated samples clearly improved the friction properties compared to the uncoated substratum. Wear rate,  $1.1 \times 10^{-7} \text{ mm}^3/\text{Nm}$ , was observed for coating surface.
- V) The adhesion and proliferation of Osteoblast cells on coating surface was enhanced. It is verified that the bioactivity of the chitosan was not damaged during the process of layer by layer deposition.



(a) Rate of proliferation of MC3T3-E1 cells



(b) SEM of cells on Co-Cr-Mo



(c) SEM of cells on Co-CS

Fig. 16. MTT and SEM morphologies of MC3T3-E1 cells on Co-Cr-Mo and Co-CS.

These results suggest the covalently grafted chitosan coatings are mainly able to have potential application in the cobalt matrix orthopedic implants.

#### Acknowledgement

The authors acknowledge the joint financial support from the National Natural Science Foundation of China (51605370 and 51475358), Postdoctoral Science Foundation of Shaanxi Province (2017BSHEDZZ122), China Postdoctoral Science Foundation funded project (2016M602802) and the Natural Science Fund of Shaanxi Province (2017JQ5009). We thank Mr Ren at instrumentanalysis center of Xi'an Jiaotong University for his assistance with SEM analysis.

#### References

- [1] Cobb AG, Schmalzreid TP. The clinical significance of metal ion release from cobalt-chromium metal-on-metal hip joint arthroplasty. *Proc. IME H J. Eng. Med.* 2006;220:385–98.
- [2] Shetty VD, Villar RN. Development and problems of metal-on-metal hip arthroplasty. *Proc. IME H J. Eng. Med.* 2006;220:371–7.
- [3] Martinez-Nogues V, Nesbitt JM, Wood RJK, Cook RB. Nano-scale wear characterization of CoCrMo biomedical alloys. *Tribol Int* 2016;93:563–72.
- [4] Wooley PH, Schwarz EM. Aseptic loosening. *Gene Ther* 2004;11:402–7.
- [5] Affatato S, Spinelli M, Zavalloni M, Mazzega-Fabbro C, Viceconti M. Tribology and total hip joint replacement: current concepts in mechanical simulation. *Med Eng Phys* 2008;30:1305–17.
- [6] Sinnott-Jones P, Wharton J, Wood R. Micro-abrasion–corrosion of a CoCrMo alloy in simulated artificial hip joint environments. *Wear* 2005;259:898–909.
- [7] Liang H, Shi B, Fairchild A, Cale T. Applications of plasma coatings in artificial joints: an overview. *Vacuum* 2004;73:317–26.
- [8] Qin L, Lin P, Zhang Y, Dong G, Zeng Q. Influence of surface wettability on the tribological properties of laser textured Co-Cr-Mo alloy in aqueous bovine serum albumin solution. *Appl Surf Sci* 2013;268:79–86.
- [9] Guo J, Li Y, Lu H, Qin L, Li Y, Dong G. An effective method of edge deburring for laser surface texturing of Co-Cr-Mo alloy. *Int J Adv Manuf Technol* 2018;94:1491–503.
- [10] Qin L, Wu H, Guo J, Feng X, Dong G, Shao J, et al. Fabricating hierarchical micro and nano structures on implantable Co-Cr-Mo alloy for tissue engineering by one-step laser ablation. *Colloids Surfaces B Biointerfaces* 2018;161:628–35.
- [11] Dearnaley G, Arps JH. Biomedical applications of diamond-like carbon (DLC) coatings: a review. *Surf Coating Technol* 2005;200:2518–24.
- [12] Patale RL, Patravale VB. O,N-carboxymethyl chitosan–zinc complex: a novel chitosan complex with enhanced antimicrobial activity. *Carbohydr Polym* 2011;85:105–10.
- [13] Khutoryanskiy VV. Advances in mucoadhesion and mucoadhesive polymers. *Macromol Biosci* 2011;11:748–64.
- [14] Smart JD. The basics and underlying mechanisms of mucoadhesion. *Adv Drug Deliv Rev* 2005;57:1556–68.
- [15] Metikoš-Huković M, Babić R. Passivation and corrosion behaviours of cobalt and cobalt–chromium–molybdenum alloy. *Corrosion Sci* 2007;49:3570–9.
- [16] Khademhosseini A, Suh KY, Yang JM, Eng G, Yeh J, Levenberg S, et al. Layer-by-layer deposition of hyaluronic acid and poly-L-lysine for patterned cell co-cultures. *Biomaterials* 2004;25:3583–92.
- [17] Feng Z, Yan F. Preparation and tribological studies of nanocomposite films fabricated using spin-assisted layer-by-layer assembly. *Surf Coating Technol* 2008;202:3290–7.
- [18] Roessler S, Zimmermann R, Scharnweber D, Werner C, Worch H. Characterization of oxide layers on Ti6Al4V and titanium by streaming potential and streaming current measurements. *Colloids Surfaces B Biointerfaces* 2002;26:387–95.
- [19] Biesinger MC, Payne BP, Grosvenor AP, Lau LWM, Gerson AR, Smart RSC. Resolving surface chemical states in XPS analysis of first row transition metals, oxides and hydroxides: Cr, Mn, Fe, Co and Ni. *Appl Surf Sci* 2011;257:2717–30.
- [20] Fan Z, Wang J, Wang Z, Li Z, Qiu Y, Wang H, et al. Casein phosphopeptide-bio-functionalized graphene biocomposite for hydroxyapatite biomimetic mineralization. *J Phys Chem C* 2013;117:10375–82.
- [21] Isabel Castellanos M, Zenses A-S, Grau A, Carlos Rodriguez-Cabello J, Javier Gil F, Maria Manero J, et al. Biofunctionalization of REDV elastin-like recombinamers improves endothelialization on CoCr alloy surfaces for cardiovascular applications. *Colloids Surfaces B Biointerfaces* 2015;127:22–32.
- [22] Irie H, Washizuka S, Yoshino N, Hashimoto K. Visible-light induced hydrophilicity on nitrogen-substituted titanium dioxide films. *Chem Commun* 2003;1298–9.
- [23] Leyland A, Matthews A. On the significance of the H/E ratio in wear control: a nanocomposite coating approach to optimised tribological behaviour. *Wear* 2000;246:1–11.
- [24] Saikko V, Calonius O, Keranen J. Effect of slide track shape on the wear of ultra-high molecular weight polyethylene in a pin-on-disk wear simulation of total hip prosthesis. *J Biomed Mater Res B Appl Biomater* 2004;69B:141–8.
- [25] Jedrzejczak A, Kolodziejczyk L, Szymanski W, Piwonski I, Cichowski M, Kiselewska A, et al. Friction and wear of a-C:H:SiOx coatings in combination with AISI 316L and ZrO2 counterbodies. *Tribol Int* 2017;112:155–62.
- [26] Todorovic P, Tadic B, Vukelic D, Jeremic M, Randjelovic S, Nikolic R. Analysis of the influence of loading and the plasticity index on variations in surface roughness between two flat surfaces. *Tribol Int* 2015;81:276–82.
- [27] Att W, Takeuchi M, Suzuki T, Kubo K, Anpo M, Ogawa T. Enhanced osteoblast

- function on ultraviolet light-treated zirconia. *Biomaterials* 2009;30:1273–80.
- [28] Anthonen MW, Varum KM, Smidsrod O. Solution properties of chitosans - conformation and chain stiffness of chitosans with different degrees of N-ACETYLATION. *Carbohydr Polym* 1993;22:193–201.
- [29] Lin L, Schlarb AK. The roles of rigid particles on the friction and wear behavior of short carbon fiber reinforced PBT hybrid materials in the absence of solid lubricants. *Tribol Int* 2018;119:404–10.
- [30] Cao HM, Zhou X, Li XY, Lu K. Friction mechanism in the running-in stage of copper: from plastic deformation to delamination and oxidation. *Tribol Int* 2017;115:3–7.
- [31] Banaszkiewicz PA. Effect of femoral head size on wear of the polyethylene acetabular component. *Classic papers in orthopaedics*. Springer; 2014. p. 101–4.
- [32] HUNG J-P, WU JS-S. A comparative study on wear behavior of hip prosthesis by finite element simulation. *Biomed Eng: Appl, Basis Commun* 2002;14:139–48.
- [33] Lee S, Muller M, Ratoi-Salagean M, Voros J, Pasche S, De Paul SM, et al. Boundary lubrication of oxide surfaces by Poly(L-lysine)-g-poly(ethylene glycol) (PLL-g-PEG) in aqueous media. *Tribol Lett* 2003;15:231–9.
- [34] Lee S, Muller M, Rezwan K, Spencer ND. Porcine gastric mucin (PGM) at the water/poly(dimethylsiloxane) (PDMS) interface: influence of pH and ionic strength on its conformation, adsorption, and aqueous lubrication properties. *Langmuir* 2005;21:8344–53.
- [35] Lavielle L. Electric-field effect on the friction of a polyethylene terpolymer film on a steel substrate. *Wear* 1994;176:89–93.
- [36] Luo JB, Shen MW, Wen SZ. Tribological properties of nanoliquid film under an external electric field. *J Appl Phys* 2004;96:6733–8.
- [37] Mahmoud MM, Mohamed MK, Ali WY. Tribological behaviour of lubricated surfaces under application of electric current. *Proc. IME J. J. Eng. Tribol.* 2010;224:73–9.
- [38] Xie GX, Li G, Luo JB, Liu SH. Effects of electric field on characteristics of nano-confined lubricant films with ZDDP additive. *Tribol Int* 2010;43:975–80.